Separation and Purification Technology 370 (2025) 133148

Contents lists available at ScienceDirect

Separation and Purification Technology

journal homepage: www.elsevier.com/locate/seppur

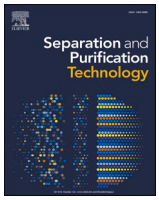

Pilot test and process modification of CO_2 chemical absorption for top gas recycling-oxygen blast furnace

Ying Xie [a], Zhixiang Xia [a], Chao Li [a], Man Mou [a], Ximing Hu [b], Wei Chen [b], Xiaoming Xu [c], Yang Xia [c], Zihao Liu [c], Mengxiang Fang [a,*]

[a] State Key Laboratory of Clean Energy Utilization, Zhejiang University, Hangzhou, China
[b] Qingshanhu Energy Research Center, Zhejiang University, Hangzhou, China
[c] Wuhan City Environment Protection Engineering Limited Company, Wuhan, China

ARTICLE INFO

Keywords:
Pilot test
Process modification
Top gas recycling-oxygen blast furnace
Steel industry
Regeneration energy

ABSTRACT

The steel industry contributes approximately 7–9 % of global anthropogenic CO_2 emissions. Chemical absorption is a promising strategy for reducing steel industry carbon emissions. MAA, a novel amine blend primarily composed of methyldiethanolamine (MDEA) and 2-(Piperazin-1-yl) ethanamine (AEP), exhibits potential but lacks industrial-scale validation. Focusing on the blast furnace (BF)-basic oxygen furnace steelmaking process, this study conducted pilot tests with MAA and 30 wt% MEA for BF gas (20 vol% CO_2) and top gas recycling-oxygen blast furnace (TGR-OBF) gas (35 vol% CO_2) and studied process modifications. The results showed that after 200 h of stable operation, MAA achieved optimal CO_2 capture from BF gas at a liquid-to-gas ratio of 8 L/Nm^3, with a regeneration energy of 2.47 GJ/t CO_2, compared to 3.78 GJ/t CO_2 for 30 wt% MEA. MAA achieved a regeneration energy of 1.81 GJ/t CO_2 for TGR-OBF gas, 26.72 % lower than that for BF gas. Absorber intercooling reduced regeneration energy by 8.86 %. Among the process modifications, directing 10 % of the rich solution to a flash evaporator for semi-lean solution recycling back to the middle of the absorber, with the remaining 90 % undergoing thermal regeneration in the stripper, demonstrated the lowest regeneration energy for TGR-OBF. This modification reduced MAA regeneration energy by 5.52 %. Additionally, two-stage water scrubbing effectively controlled amine emissions from the 10 Nm^3/h pilot plant, reducing MAA emissions to 17.83 mg/Nm^3 after the second stage. MAA exhibited excellent adaptability to BF and TGR-OBF gases, achieving 90 % CO_2 removal efficiency with a minimum regeneration energy of 1.71 GJ/t CO_2. The findings highlight the potential for the large-scale application of MAA in the steel industry to significantly reduce CO_2 emissions.

1. Introduction

The steel industry accounts for approximately 7–9 % of global anthropogenic CO_2 emissions [1], driven by the combustion of fossil fuels and chemical reactions involved in the steelmaking process. Particularly, large volumes of carbon dioxide are generated during the blast furnace (BF)-basic oxygen furnace and electric arc furnace steelmaking processes [2,3]. Reducing these emissions is crucial for achieving global carbon neutrality goals [4]. Carbon capture technology can reduce carbon emissions [5], but direct carbon capture from BF gas increases costs [6]. Consequently, researchers proposed the top gas recycling–oxygen blast furnace (TGR-OBF) [7–9]. BF gas contains 20 % CO and 20 % CO_2. By separating CO_2 from the top gas and recycling the CO back into the furnace, the calorific value of the BF gas can be improved, the reduction rate in the furnace enhanced, and the coke ratio reduced, with economic benefits [10,11] (Fig. 1).

Among carbon capture technologies, chemical absorption has garnered significant attention for controlling steel production CO_2 emissions [12]. It involves the use of amine-based solvents to capture CO_2 from the gas phase via a liquid-phase reaction and separate it by heating and desorption, enabling solvent regeneration for reuse [13]. This technology offers high absorption efficiency and relatively mature technological development [14,15]. Monoethanolamine (MEA) is the most-used absorbent in CO_2 capture, with 30 wt% MEA solution considered the benchmark for evaluating the performance of new absorbents [16–18].

However, the implementation of carbon capture technology in the steel industry presents several challenges. BF gas contains approxi-

* Corresponding author.
E-mail address: mxfang@zju.edu.cn (M. Fang).

https://doi.org/10.1016/j.seppur.2025.133148
Received 15 January 2025; Received in revised form 21 February 2025; Accepted 20 April 2025
Available online 21 April 2025

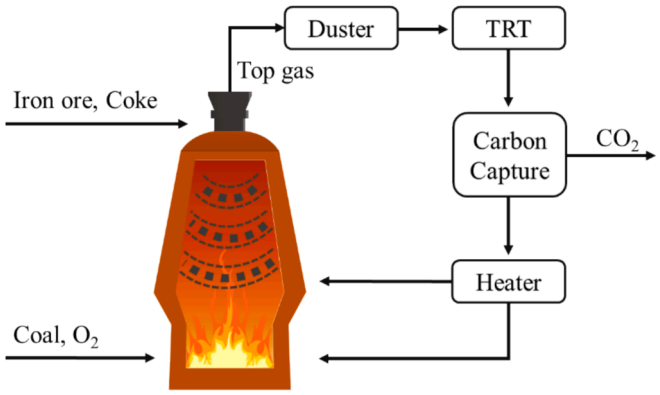

Fig. 1. Schematic diagram of TGR-OBF working principle.

mately 20 % CO_2, compared to the typical 12 % in power plant flue gas [19]. When TGR-OBF is employed, the CO_2 concentration can increase to 37.9 % [20]. High CO_2 concentrations pose a significant challenge to the capacity of absorbents. Conventional primary and secondary amines react with CO_2 to form carbamates through a 2:1 M stoichiometry (2 mol of amine per 1 mol of CO_2; Eq. (1). In contrast, tertiary amines, which cannot form carbamates, react via a 1:1 M ratio to produce bicarbonates (Eq. (2) [21]. Consequently, primary and secondary amines are less-suited for carbon capture in the steel industry. Furthermore, higher CO_2 concentrations affect amine emissions [22]. Increased energy consumption associated with absorbents also impacts process net costs [23]. Therefore, process modifications and innovations in amine formulations to reduce capture costs have become a primary research focus [24,25].

$$2RNH_2 + CO_2 \leftrightarrow RNH_3^+ + RNHCOO^- \quad (1)$$

$$R_1R_2R_3N + CO_2 + H_2O \leftrightarrow R_1R_2R_3NH^+ + HCO_3^- \quad (2)$$

Previous research on amine innovations for BF gas has focused on amine blends. Table 1 summarizes the experiments and simulations conducted on the chemical absorption of CO_2 captured from BF and TGR-OBF gases. Goto et al. [26] evaluated 2-isopropylaminoethanol (IPAE)-based amine solvents, reporting CO_2 regeneration energies of 3.1 GJ/tCO_2 at the 1 t CO_2/d test plant. Wells et al. [27] simulated the optimal liquid-to-gas ratio (L/G) and solution/CO_2 ratios of MEA absorption systems for BF gas. Tobiesen et al. [28] compared the performance of various absorbents using a rate-based closed-loop model, finding that 2-amino-2-methyl-1-propanol (AMP) and methyldiethanolamine (MDEA)/ piperazine (PZ) were energy-efficient. Dreillard et al. [29] verified that a demixing solvent could produce CO_2 at 6 bara in a CO_2 capture mini-pilot plant. Chung et al. [30] studied CO_2 capture processes employing amine (piperazine) scrubbing for TGR-OBF, achieving lower operating costs. The Bayi Steel Company of Baowu Group in China has constructed a 120,000 Nm^3/h hydrogen-rich carbon circulating BF gas carbon capture device, based on a 2500 m^3 BF [31]. Our previous study reported MAA, an amine blend primarily composed of MDEA and 2-(Piperazin-1-yl) ethanamine (AEP), as a chemical absorbent in the steel industry [32]. MAA has a similar maximum absorption rate to 30 % MEA. At CO_2 concentrations of 20 % and 35 %, the cyclic capacities of MAA were 1.57 and 1.47 times greater and the maximum regeneration rates were 2.13 and 1.92 times greater, than those of 30 wt% MEA, respectively. However, while MAA has exhibited excellent absorption and regeneration performances in the laboratory, its performance under industrial operating conditions has yet to be determined. Therefore, pilot testing of MAA is required to validate its potential for industrial applications.

Table 1
Research on chemical absorption of BF and TGR-OBF gases.

Gas	CO_2 concentration	Pressure	Method	Absorbent	Reference
BF gas	20 %	1 bar	Pilot test	RITE-B	[26]
BF gas	24 %	Unknown	Simulation	MEA	[27]
BF gas	23 %	2.53 bar	Simulation	AMP	[28]
TGR-OBF gas	36 %	2.53 bar	Simulation	MDEA/PZ	[28]
TGR-OBF gas	37.04 %	6 bar	Mini-pilot tests	DMX	[29]
TGR-OBF gas	36 %	2.5 bar	Simulation	PZ	[30]
TGR-OBF gas	33.5 %	0.85 Mpa	Pilot test	Unknown	[31,33]
BF gas	20 %	1 Mpa	Pilot test	MAA	This study
TGR-OBF gas	35 %	0.8 Mpa	Pilot test	MAA	This study

Researchers have validated the effectiveness of several process modifications, such as absorber intercooling (AIC) [34–36], rich solvent splitting [37–39], and lean vapor compression [40–43]. Cousins et al. [36] simulated a 100 kg/h pilot plant and found that AIC provided a 6.4 % saving in reboiler duty. Dubois et al. [44] found that rich solution recycling (RSR) allows for increasing the CO_2 loading of the rich solution leading to a decrease in the regeneration energy from 3.15 to 2.95 GJ/tCO_2. Le Moullec et al. [45] noted that rich solution flashing (RSF) had a lower impact on the capture system when the pressure difference between the absorber and stripper was small (0–2 bar). They believed that RSF is suitable when the absorber operates at a pressure significantly higher than atmospheric pressure. The combination of different process modifications can further reduce the regeneration energy [46]. Bayi Steel Company found that in the TGR-OBF carbon capture process, the absorber pressure can reach 0.85 MPa [31,33], thus necessitating process modifications. Currently, there is a notable absence of research focused on process modification for the chemical absorption of TGR-OBF.

This study aimed to validate the industrial potential of MAA for CO_2 capture from BF and TGR-OBF gases through pilot testing. Key parameters such as cyclic capacity, regeneration energy, and amine emissions were tested. In addition, process modifications suitable for carbon capture in the TGR-OBF and their combinations were explored, filling a gap in this field.

2. Experiments

2.1. Chemicals

All chemicals used were industrial grade. MEA (purity 99 %), MDEA (purity 99 %), and AEP (purity 99 %) were purchased from Aladdin Biochemical Technology Co. Ltd., Shanghai, China. CO_2 (99.999 % pure) was purchased from Hangzhou Jingong GAS Co. Ltd., Hangzhou, China. Deionized water was used throughout the experiments.

2.2. CO_2 capture pilot plant

The continuous absorption and regeneration performance of the different absorbents was tested in a pilot plant (Fig. 2). The experimental conditions for BF and TGR-OBF gases were based on past studies (Table 1). The BF gas had a pressure of approximately 0.1 MPa and CO_2 concentration of 20 %. Test conditions for the TGR-OBF gas were 0.8 MPa pressure and 35 % CO_2 concentration.

2.2.1. Process flow

In the BF gas test, CO_2 was controlled by a CO_2 cylinder and air was controlled by a compressor (Fig. 3). Mass flow meters adjusted the gas

Fig. 2. CO_2 capture pilot plant: (a) first floor (preprocessing unit); (b) second floor (absorption and desorption unit); and (c) third floor (water washing and flash evaporation unit).

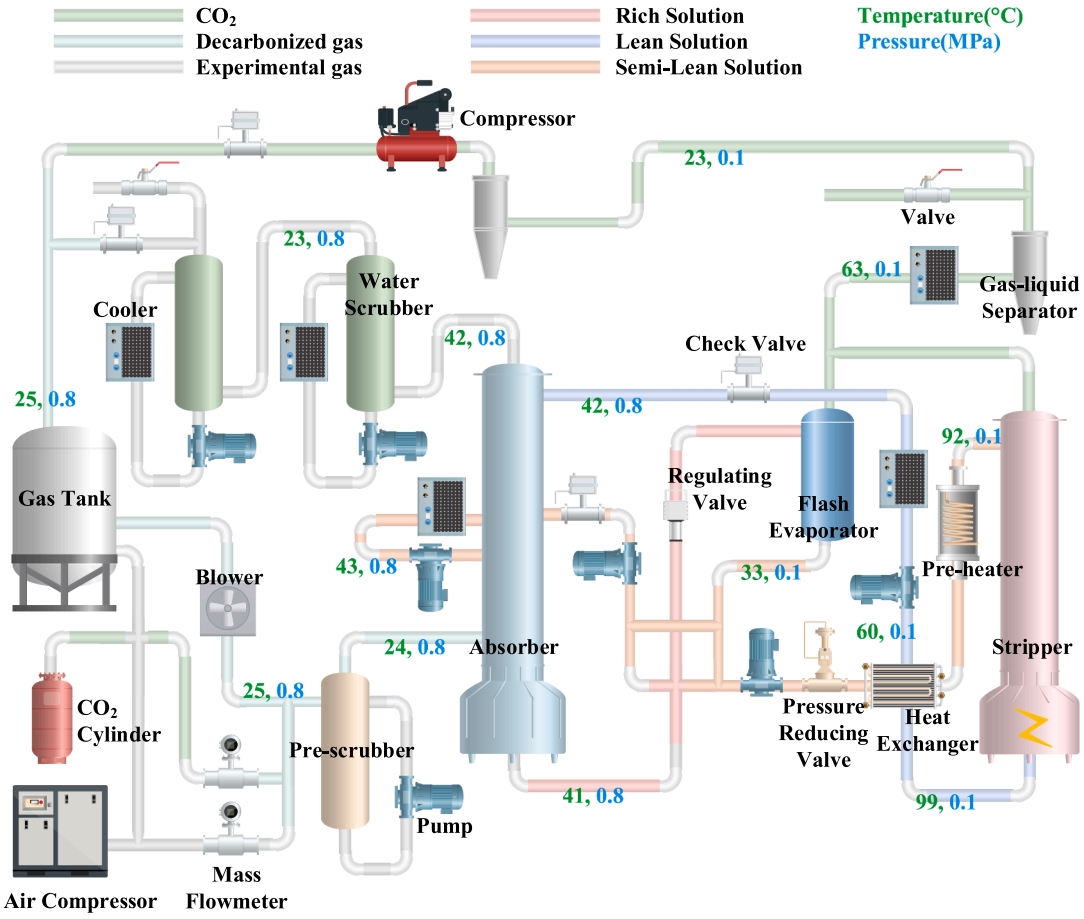

Fig. 3. Process flow diagram for CO_2 capture pilot plant (with typical temperature and pressure data from TGR-OBF gas tests).

composition to simulate BF gas with a CO_2 concentration of 20 % or 35 %. After passing through a pre-scrubber, the simulated BF gas entered the absorber for decarbonization. The gas entered from the bottom in countercurrent contact with the lean solvent flowing into the absorber from the top, removing the CO_2 in the gas. The tower temperature was reduced and removal efficiency improved using an AIC process. The decarbonized gas was cooled in two water scrubbers, simultaneously removing volatile amines while maintaining the water balance of the

system. The temperature of the cooling water was controlled using an electric cooler.

After absorbing CO_2, the rich solution was pumped from the bottom of the absorber into a heat exchanger, where it underwent heat exchange with the lean solution. It was then preheated to approximately 90 °C before being sent to the stripper. The desorbed lean solution was cooled before being returned to the top of the absorber to complete solvent circulation.

The CO_2-rich regeneration gas from the top of the stripper was cooled before separation in a gas–liquid separator, yielding concentrated CO_2. The separated condensate was returned to the stripper.

The design parameters of the pilot plant are listed in Table 2. Table 3 provides the tower equipment specifications, all of which employ θ ring packing (Fig. 4).

2.2.2. System stability verification

System operation was considered stable when the regeneration gas flow rate, solution flow rate, and tower temperature stabilized within 1 h (with a deviation of 5 %).

CO_2 mass balance was investigated to verify measurement consistency. Three CO_2 flow rates were calculated: absorption-side CO_2 flow rate in the experimental gas, regeneration-side CO_2 flow rate in the regeneration gas, and solution-side CO_2 transfer rate in the solution. The results indicate that the CO_2 transfer rates on the absorption, solution, and regeneration sides were highly consistent, with deviations within 10 % (Fig. 5), confirming test stability.

The temperature of the rich solution fluctuated around 93 °C, while the temperature of the lean solution fluctuated around 108 °C, maintaining a temperature approach of 15 °C (Fig. 6). Under actual industrial conditions, this temperature approach can be readily achieved using a heat exchanger.

2.2.3. Energy-saving process

Four energy-saving processes were tested for the pilot plant (Fig. 7).

2.2.3.1. Absorber intercooling. Since the CO_2 absorption process is exothermic, the absorber temperature increased, particularly in the lower section of the absorber, primarily governed by thermodynamic control. This adversely affected the mass-transfer driving force for CO_2 absorption, limiting rich solution loading at the tower bottom. AIC effectively mitigated the limitation caused by temperature increase, enabling increased CO_2 loading of the rich solution (Fig. 7**(a)**).

2.2.3.2. Rich solution flashing. To recover the system heat more effectively and reduce the energy input to the stripper, rich solution flashing (RSF) utilized the pressure from high-pressure absorption conditions (Fig. 7**(a)**). Under RSF, the high-pressure rich solution was directly introduced into an atmospheric pressure flash evaporator, where the solubility of CO_2 in the solvent under high pressure differed significantly from that under atmospheric pressure. The rapid pressure drop caused CO_2 to desorb, enabling partial regeneration of the rich solution, forming a semi-lean solution. The semi-lean solution was then fed into the stripper for thermal regeneration, reducing the regeneration energy. Fig. 8 illustrates the structure of the flash evaporator, where the solvent achieves gas–liquid separation through atomizing nozzles.

Table 2
Key operating parameters of the CO_2 capture pilot plant.

Parameter	Unit	Value
Gas flow rate	Nm^3/h	10
Gas temperature before entering the system	℃	20–25
Gas temperature after leaving the system	℃	20–25
CO_2 concentration	Vol%	20–35
CO_2 removal efficiency	%	≥90
Solution flow rate	kg/h	50–120
Electric heating power of the stripper	kW	12
Temperature of the stripper kettle	℃	105–115
Preheating temperature of the stripper	℃	88–92
Pump power	W	450
Compressor power	kW	1.1

Table 3
Column design specifications for the pilot plant.

Parameter	Column inner diameter /mm	Packing height /m	Packing type	Packing material
Absorber	100	2.5	6 mm θ ring	Stainless steel
Stripper	80	2	4 mm θ ring	Stainless steel
Pre-scrubber	100	0.5	6 mm θ ring	Stainless steel
Water scrubber I	100	0.5	6 mm θ ring	Stainless steel
Water scrubber II	100	0.5	6 mm θ ring	Stainless steel
Flash evaporator	800	0.25	6 mm θ ring	Stainless steel

2.2.3.3. Semi-lean solution recycling. Under RSF, the semi-lean solution undergoes partial CO_2 desorption. Recycling the semi-lean solution back into the absorber allows CO_2 to be reabsorbed (Fig. 7**(a)**). SSR reduces the temperature in the absorber, increases the rich solution loading, and improves energy efficiency.

2.2.3.4. Rich solution recycling. When the CO_2 concentration was relatively high, such as 35 %, to enhance CO_2 removal efficiency the energy input to the stripper needed to be significantly increased by reducing the lean solution loading and increasing the solvent cyclic capacity. However, this resulted in higher regeneration energy. Recycling a portion of the rich solution back to the mid-section of the absorber had a dual purpose (Fig. 7**(b)**); it extended the absorption reaction time and improved the rich solution loading.

2.3. Measurement methods

The CO_2 concentration, loading, removal efficiency, regeneration energy, and amine emissions were tested and calculated. The solution flow rate in the pilot plant was measured using an electromagnetic flow meter. The gas flow rate was monitored using a vortex flow meter. Data on the flow rate, temperature, pressure, and liquid level were displayed on the system control interface.

2.3.1. CO_2 concentration

The inlet and decarbonized outlet gases from the absorber were routed through a drying tube and the CO_2 concentration was analyzed using a portable infrared analyzer (GXH-3011E; Huayun Analytical Instrument Research Institute Co. Ltd., Beijing, China). The instrument had a linearity error of ≤±2% F.S., and repeatability of ≤±1% F.S. The analyzer was calibrated before testing using standard gases.

2.3.2. CO_2 loading

Solvent CO_2 loading was measured by acid-base titration:

$$\alpha = \frac{V_{CO2}}{V_0} \times \frac{P}{R \times T} \times 10^{-3} \quad (3)$$

where α is the CO_2 loading of the solvent (in mol/L), V_{CO2} is the volume of CO_2 evolved as measured by titration (in ml), V_0 is the volume of the solution used in the titration (in ml), P is pressure (in Pa), T is temperature (in K), and R is the universal gas constant (in 8.314 J/(mol·K).

2.3.3. CO_2 removal efficiency

It was assumed that gases such as N_2 and O_2 did not react with the

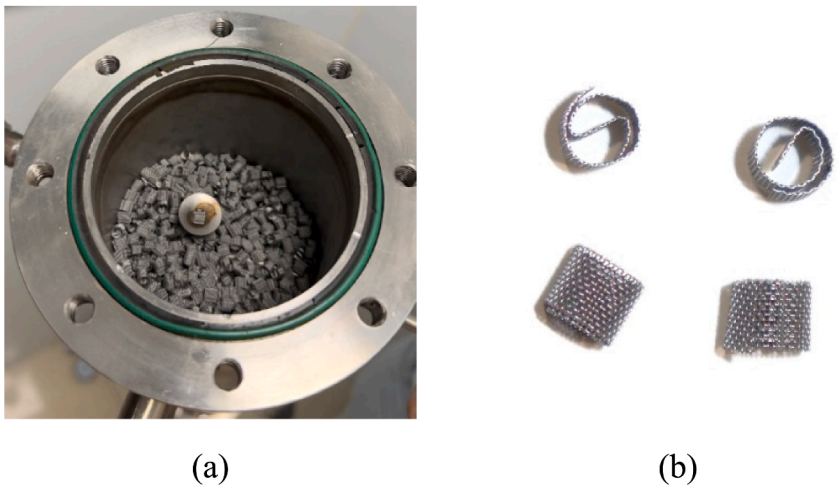

Fig. 4. Photograph of θ ring packing: (a) cross section of the stripper and (b) θ ring packing.

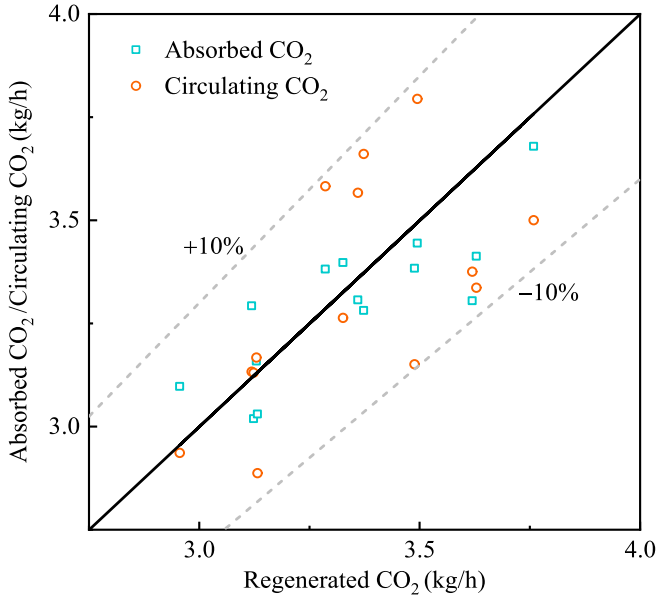

Fig. 5. Errors in the three CO_2 flow rates.

solvent. The CO_2 removal efficiency was calculated as follows:

$$\psi = \left[1 - \frac{(1 - C_{in}) \times C_{out}}{C_{in} \times (1 - C_{out})}\right] \times 100\% \quad (4)$$

where C_{in} is the CO_2 concentration at the inlet and C_{out} is the CO_2 concentration at the outlet of the absorber.

2.3.4. Regeneration energy

The regeneration energy was calculated based on the amount of CO_2 produced and the energy consumption of the electric heater in the stripper kettle, and the electric heater was adjusted to maintain a stable stripper kettle temperature while ensuring a CO_2 removal efficiency above 90 %:

$$Q_{reg} = \frac{(E^* - E_0) \times 3.6 \times 10^6}{\Delta t \times q_{CO2}} \quad (5)$$

where Q_{reg} is the regeneration energy (in GJ/t CO_2), q_{CO2} is the CO_2 mass flow rate during regeneration (in t/h), E_0 is the initial energy meter reading (in kW•h), E^* is the ending energy meter reading (in kW•h),

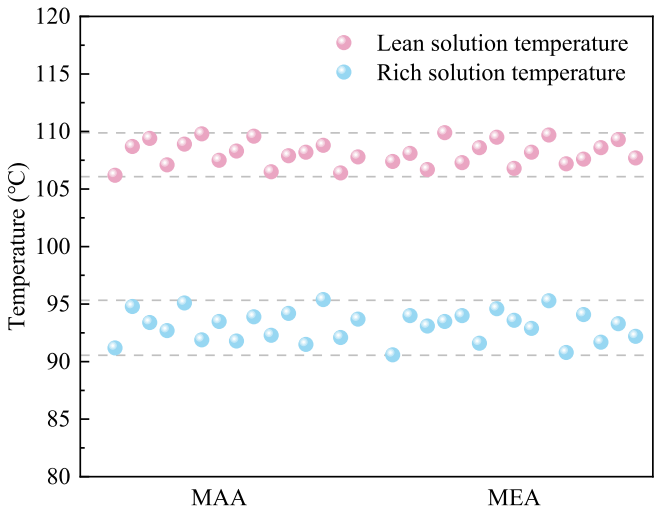

Fig. 6. Temperature of lean and rich solutions at the outlet and inlet of the stripper in multiple tests.

$E^* - E_0$ represents the net energy consumption of the electric heater in the stripper kettle, and Δt is the time duration of the test (in h). The cumulative electrical energy input $E^* - E_0$ was measured using a three-phase digital energy meter (Accuracy Class 0.5 %) installed at the power supply terminal of the stripper heater. The meter recorded active energy consumption (kW•h) at 1 s intervals. Initial (E_0) and final (E^*) readings were recorded after the system reached a steady state.

The mass flow rate of the regeneration gas was calculated as

$$q_{CO2} = \frac{Q_{CO2} \times P_{CO2} \times (1 - w_{H2O}) \times MW_{CO2}}{R \times T_{CO2}} \times 10^{-6} \quad (6)$$

where Q_{CO2} is the actual volumetric flow rate of the regeneration gas (in m^3/h), P_{CO2} is the regeneration gas pressure (in Pa), T_{CO2} is the regeneration gas temperature (in K), R is the universal gas constant (in 8.314 J/(mol·K)), w_{H2O} is the mass fraction of water in the regeneration gas (dimensionless), and MW_{CO2} is the molar mass of CO_2 (in 44 g/mol).

2.3.5. Amine emissions

The amine emissions were tested using a constant-flow-rate sampling method combined with cation chromatography (Dionex Aquion ICS-5000; Thermo Fisher Scientific, Waltham, MA, USA) (Fig. 9). Volatile

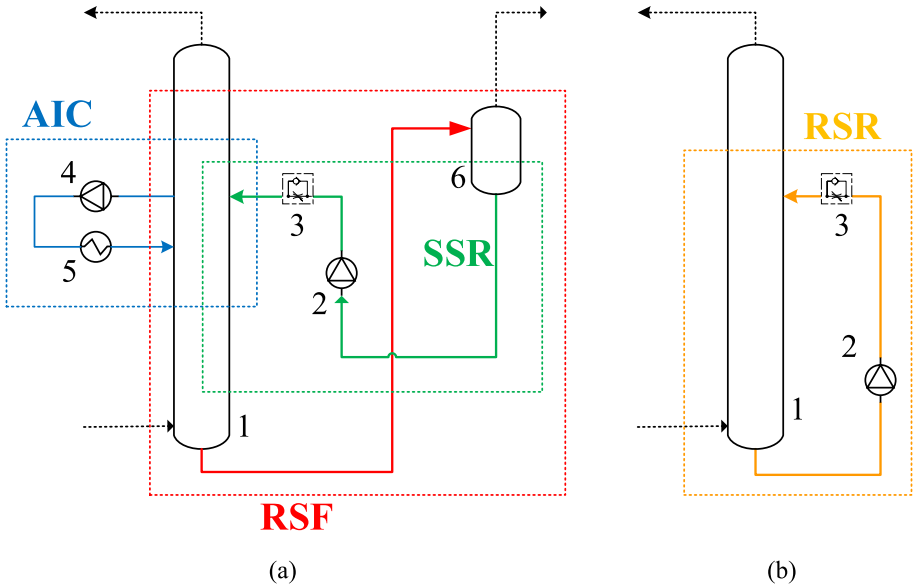

Fig. 7. Energy-saving process flow diagram for the pilot plant: (a) absorber intercooling process (AIC) in blue, rich solution flashing process (RSF) in red, and semi-lean solution recycling process (SSR) in green; (b) rich solution recycling (RSR) process in orange (1: absorber; 2: semi-lean solution pump; 3: check valve; 4: intercooling pump; 5: intercooler; 6: flash evaporator).

Fig. 8. Flash evaporator structural details: (a) full assembly; (b) cross-section; and (c) atomizing nozzle.

amine emissions were calculated as follows:

$$E_{am} = \frac{C_{am} \times V}{Q_S \times \Delta t} \bullet \frac{P_0 \times T}{P \times T_0} \quad (7)$$

where E_{am} is the amine emission (in mg/Nm^3), C_{am} is the amine concentration in the acid wash solution measured by cationic chromatography (in mg/L), V is the volume of the acid wash solution (in mL), Q_S is the sampling pump flow rate (in L/min), Δt is the sampling time (in min),P is the experimental pressure (in Pa), T is the experimental temperature (in K), P_0 is standard atmospheric pressure (101325 Pa), and T_0 is the ideal gas temperature (273.15 K).

3. Results and discussion

The experiment was conducted over two months at the pilot plant. The tests were performed using two absorbents, MAA and 30 wt% MEA (hereinafter referred to as MEA), with the solvents operating stably for over 200 h.

3.1. CO_2 capture performance under BF conditions

The BF gas test investigated the loads under steady-state conditions. Fig. 10 illustrates the variations in the lean solution loading and cyclic capacity with the liquid-to-gas (L/G), where the total height of the stacked bar chart represents rich solution loading. Notably, solution loading is the CO_2 loading per unit volume of solution (in mol/L), and

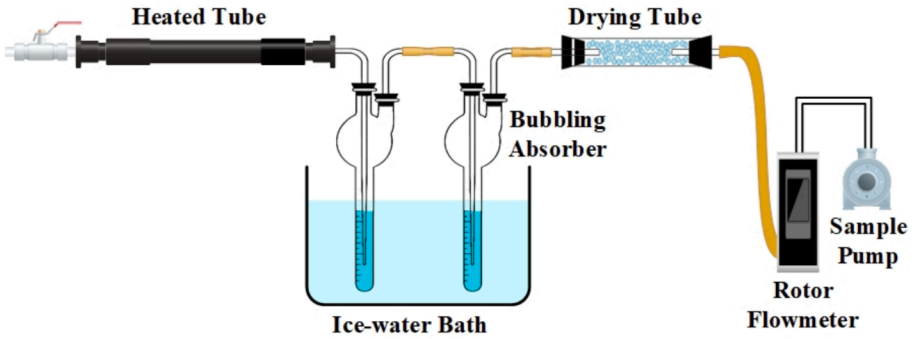

Fig. 9. Experimental setup for amine emission measurements.

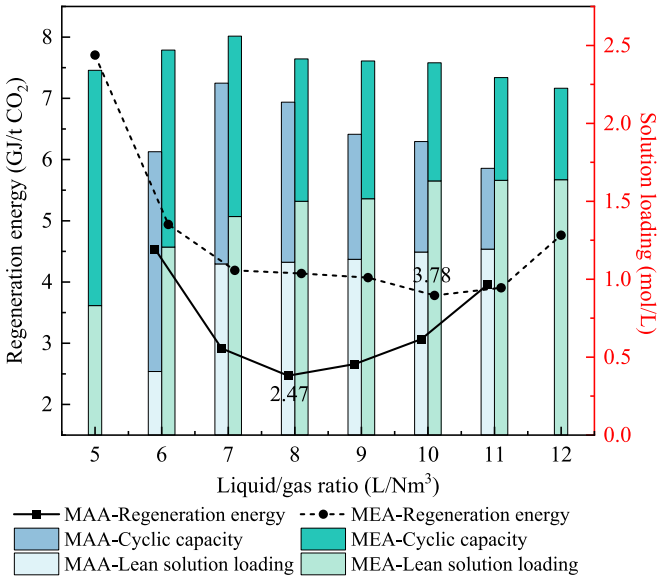

Fig. 10. Variations in regeneration energy and solution loading with L/G for MAA and MEA during the 10 Nm^3/h BF gas tests.

cyclic capacity is the difference between the rich and lean solution loading (in mol/L). Lean solution loading increased with L/G, whereas cyclic capacity decreased. This occurred because, as L/G increased, the solution circulation rate increased, while the gas flow rate remained constant. Consequently, the CO_2 absorption required per unit of solution decreases, leading to a decline in the cyclic capacity. Since reducing the lean solution loading is challenging and energy-intensive, maintaining a relatively high rich solution loading is preferred. Consequently, the lean solution loading increased. The MAA and MEA cyclic capacity maxima were 1.41 and 1.51 mol/L, respectively. The rich solution loading for MAA ranged from 1.71 to 2.26 mol/L, while that for MEA ranged from 2.23 to 2.56 mol/L.

The regeneration energies of both MAA and MEA exhibited the same trend with changing L/G: the regeneration energy first decreased and then increased as L/G increased (Fig. 10). When the gas flow rate remains constant and the solution circulation rate is too low, resulting in a low L/G, the required lean solution loading must be significantly reduced to achieve the desired CO_2 removal efficiency. This leads to higher regeneration energy. Conversely, when the L/G is too high, the regeneration heat required increases substantially, increasing regeneration energy demand. MAA achieved its lowest regeneration energy of 2.47 GJ/t CO_2 at an L/G of 8 L/Nm^3, while MEA reached its minimum regeneration energy of 3.78 GJ/t CO_2 at an L/G of 10 L/Nm^3. The regeneration energy of MAA was 34.66 % lower than that of MEA. At the minimum regeneration energy, the cyclic capacity was 1.03 mol/L for MAA and 0.76 mol/L for MEA. For MAA, in the low L/G range (6–8 L/Nm^3), the regeneration energy decreased from 4.54 to 2.47 GJ/t CO_2, while in the high L/G range (8–11 L/Nm^3), it increased from 2.47 to 3.96 GJ/t CO_2. Similarly, for MEA, in the low L/G range (5–10 L/Nm^3), the regeneration energy decreased from 7.71 to 3.78 GJ/t CO_2, and in the high L/G range (10–12 L/Nm^3), it increased from 3.78 to 4.76 GJ/t CO_2. The significant difference in the optimal L/G between MAA and MEA was attributed to the distinct loading capacities of the two absorbents, as well as differences in their regeneration rates, energy requirements, and reaction heats.

3.2. CO_2 capture performance under TGR-OBF conditions

During the TGR-OBF gas tests, the rich solution in the absorber was subjected to a pressure of 0.8 MPa, whereas the titration experiments to measure solution loading were conducted at atmospheric pressure. When the rich solution was sampled during testing, significant CO_2 evolution was observed, making it impossible to accurately measure high-pressure-rich solution loading in the absorber. Fig. 5 demonstrates a strong consistency in CO_2 transfer rates between the absorption side, solution side, and regeneration side. Based on this observation, the experiment assumed that under TGR-OBF gas conditions, the CO_2 transfer rate in the solution equaled the CO_2 flow rate at the regeneration gas. Therefore, the CO_2 transfer rate in the solution was calculated. Subsequently, the rich solution loading was determined based on the flow rates of the rich and lean solutions and lean solution loading.

To ensure stable testing conditions, CO_2 or air was promptly supplied when the absorber pressure and CO_2 concentration changed because of sampling and other system operations, maintaining the pressure within 0.75–0.85 MPa and the CO_2 concentration within 34–36 %.

Fig. 11 illustrates the variations in the lean solution loading and cyclic capacity with L/G, where the total height of the stacked bar chart represents rich solution loading. The cyclic capacity of the solvent decreased as L/G increased. This decline occurred because an increase in L/G led to a higher solution circulation rate, whereas the gas flow rate remained constant, resulting in reduced CO_2 absorption per unit of solution and a decreased cyclic capacity. The maximum cyclic capacity was 2.14 mol/L for MAA and 1.61 mol/L for MEA. The rich solution loading for MAA ranged from 2.83 to 3.35 mol/L, while for MEA, it fluctuated between 3.16 and 3.41 mol/L.

The regeneration energies of MAA and MEA during the TGR-OBF gas tests followed the same trend as that of the L/G (Fig. 11). Both solvents exhibited a decrease in the regeneration energy as L/G increased, followed by an increase, with the minimum regeneration energy occurring at the inflection point. For MAA, the lowest regeneration energy of 1.81 GJ/t CO_2 was observed at an L/G of 8.5 L/Nm^3. For MEA, the lowest regeneration energy of 2.56 GJ/t CO_2 occurred at an L/G of 11 L/Nm^3, representing a 29.3 % decrease in regeneration energy for MAA compared to MEA. The cyclic capacity of MAA at the lowest regeneration energy was 2.00 mol/L, whereas that of MEA was 1.54 mol/L. For

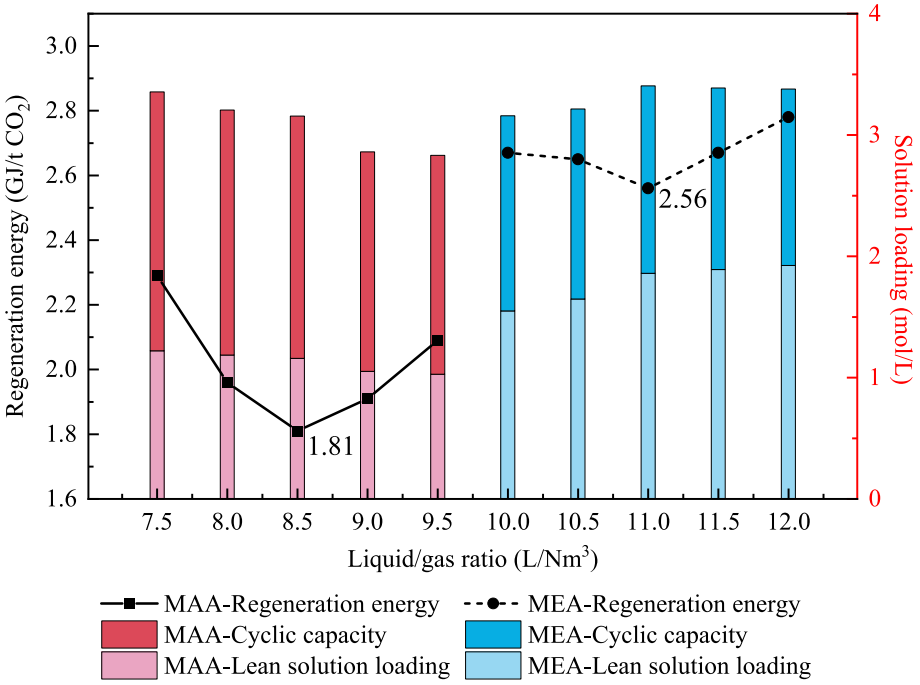

Fig. 11. Variations in solution loading and regeneration energy with L/G during the 10 Nm^3/h TGR-OBF gas tests for MAA and MEA.

MAA, within the low L/G range (7.5–8.5 L/Nm^3), the regeneration energy decreased from 2.29 to 1.81 GJ/t CO_2, while within the high L/G range (8.5–9.5 L/Nm^3), the regeneration energy increased from 1.81 to 2.09 GJ/t CO_2. For MEA, within the low L/G range (10–11 L/Nm^3), the regeneration energy decreased from 2.67 to 2.56 GJ/t CO_2, while within the high L/G range (11–12 L/Nm^3), it increased from 2.56 to 2.78 GJ/t CO_2. The difference in the L/G testing ranges for MAA and MEA was due to the different loading capacities of the two absorbents. The cyclic capacity range for MAA was 1.80–2.14 mol/L, while that for MEA was 1.45–1.61 mol/L (Fig. 12). Because MEA has a smaller cyclic capacity, a higher L/G was required to achieve over 90 % CO_2 removal efficiency.

Fig. 12 compares the regeneration energy and solution loading at the optimal L/G for MAA and MEA during the BF and TGR-OBF gas tests. Under TGR-OBF conditions, the lowest regeneration energy for MAA was 1.81 GJ/t CO_2, compared to 2.47 GJ/t CO_2 under BF conditions, a decrease of 26.72 %. For MEA, the lowest regeneration energy under TGR-OBF conditions was 2.56 GJ/t CO_2, compared to 3.78 GJ/t CO_2 under BF conditions, a decrease of 32.28 %. MAA consistently exhibited a lower regeneration energy than MEA under both test conditions. The reduction in the regeneration energy under the TGR-OBF test compared with the BF test was attributed to the higher pressure (0.8 MPa) and higher CO_2 concentration (35 %), which promoted CO_2 absorption, resulting in a higher rich solution loading. Under TGR-OBF conditions, the solution loading of MAA was 3.16 mol/L, 47.66 % higher than that under the BF conditions (2.14 mol/L). The increased CO_2 concentration required a larger cyclic capacity and a higher solution circulation rate to achieve a CO_2 removal efficiency exceeding 90 %. Under TGR-OBF conditions, the cyclic capacity of MAA was 2.00 mol/L, 94.17 % higher than that under BF conditions (1.03 mol/L). Simultaneously, the amount of regenerated CO_2 increased significantly. A higher rich solution loading reduced the need to lower the lean solution loading in the stripper, resulting in a reduction in the regeneration energy under TGR-OBF conditions.

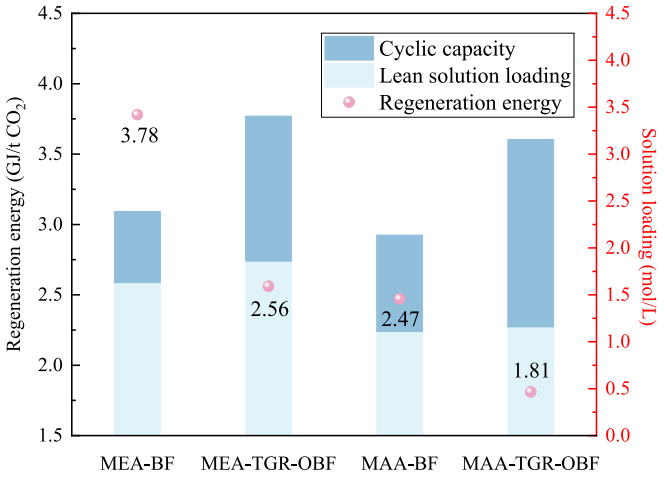

Fig. 12. Performance comparison between BF and TGR-OBF gas tests.

3.3. Process modification

3.3.1. Effect of absorber intercooling

As shown in Fig. 13, the temperature distribution along the plates ranged from 41.8 to 55.2 °C. AIC significantly reduced the solvent temperature at plates 1, 2, and 3, as well as at the absorber bottom. The lowest temperature, 42.5 °C, occurred at the bottom where no absorption reaction took place, followed by 44 °C at the third plate with intercooling. The continuous exothermic reaction between CO_2 and amine increased the temperature of the absorber. The results indicate that AIC improved the thermodynamics of the absorption process.

The regeneration energies with and without AIC were evaluated under the optimal BF gas test conditions. AIC reduced the regeneration energy of MAA and MEA, with a more pronounced effect observed for MAA (Fig. 14). Specifically, the regeneration energy consumption of MAA decreased by 8.86 % (2.71 to 2.47 GJ/t CO_2), while that of MEA decreased by 8.47 %. Given the significant energy-saving effect of AIC, this process was enabled in all subsequent tests. The cooling-water temperature and flow rate of the AIC were maintained constant throughout the tests. Based on the pilot plant scale, the cooling-water flow rate was controlled at 50 L/h, with a cooling-water temperature of 20 °C.

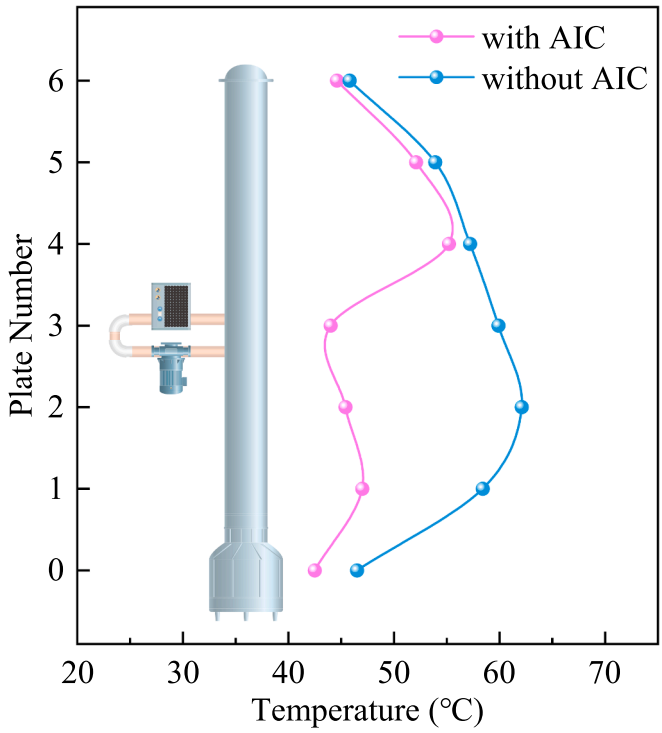

Fig. 13. Absorber temperature distribution along the plate numbers.

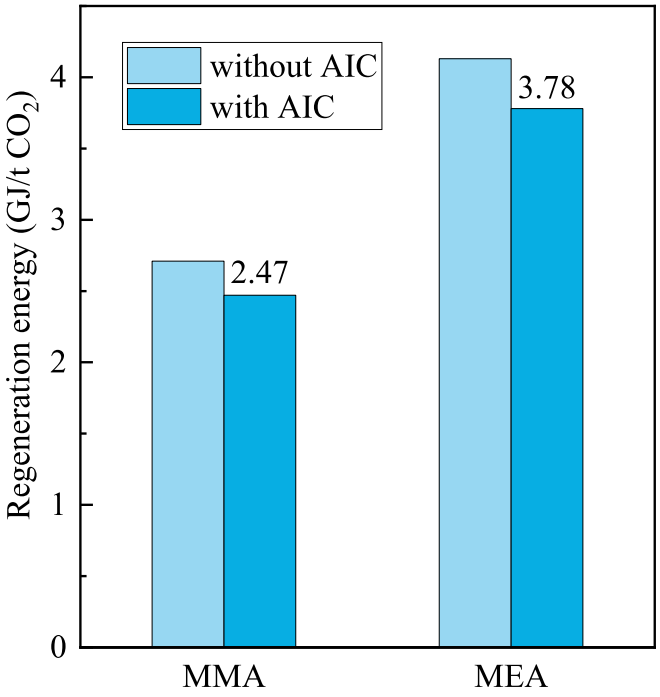

Fig. 14. Regeneration energy reduction through AIC.

3.3.2. Process modifications for TGR-OBF conditions

The study of process modifications was based on the optimal L/G of the solvents. As described in Section 2.2, the pilot plant incorporated several energy-saving processes. Based on the characteristics of the TGR-OBF gas tests, several process modification routes were designed (Table 4). As AIC reduces the regeneration energy and lowers amine emissions from the system, all tests were conducted with AIC.

Routes 1 and 2 are illustrated in Fig. 15**(a) and 15(b)**, respectively.

Table 4
Process modification routes for TGR-OBF conditions.

Route	Process Modification	Description
Route 1	RSF × Thermal desorption (TD)	The entire rich solution enters the flash evaporator for flashing, and the resulting semi-lean solution fully undergoes thermal desorption in the stripper.
Route 2	RSF × (SSR + TD) Split ratio: 5–20 %	The entire rich solution enters the flash evaporator for flashing, with 5–20 % of the resulting semi-lean solution recycled to the mid-section of the absorber. The remaining 80–95 % of the semi-lean solution undergoes thermal desorption in the stripper.
Route 3	(RSF × SSR)+ TD Split ratio: 5–20 %	5–20 % of the rich solution enters the flash evaporator for flashing, and the resulting semi-lean solution is fully recycled to the mid-section of the absorber. The remaining 80–95 % of the rich solution directly undergoes thermal desorption in the stripper.
Route 4	RSR + (RSF × TD) Split ratio: 5–20 %	The 5–20 % of the rich solution is recycled to the mid-section of the absorber. The remaining 80–95 % of the rich solution enters the flash evaporator for flashing, and the resulting semi-lean solution fully undergoes thermal desorption in the stripper.

We investigated the variation in regeneration energy with the split ratio under Route 2 to determine the optimal split ratio. Under Route 2, a split ratio of zero corresponds to Route 1. As shown in Fig. 16**(a)**, the regeneration energies for MAA and MEA initially increased, decreased, and then increased with an increasing split ratio. When the split ratio was low (5 %), the improvement in the rich solution loading compared with that under Route 1 was limited, and the semi-lean solution flow rate entering the stripper decreased. This reduction necessitated a higher cyclic capacity, requiring increased heating power to achieve the same CO_2 removal efficiency (>90 %) as achieved under Route 1. When the split ratio increased to 10 % or 15 %, the improvement in the rich solution loading became more pronounced, leading to an increase in the

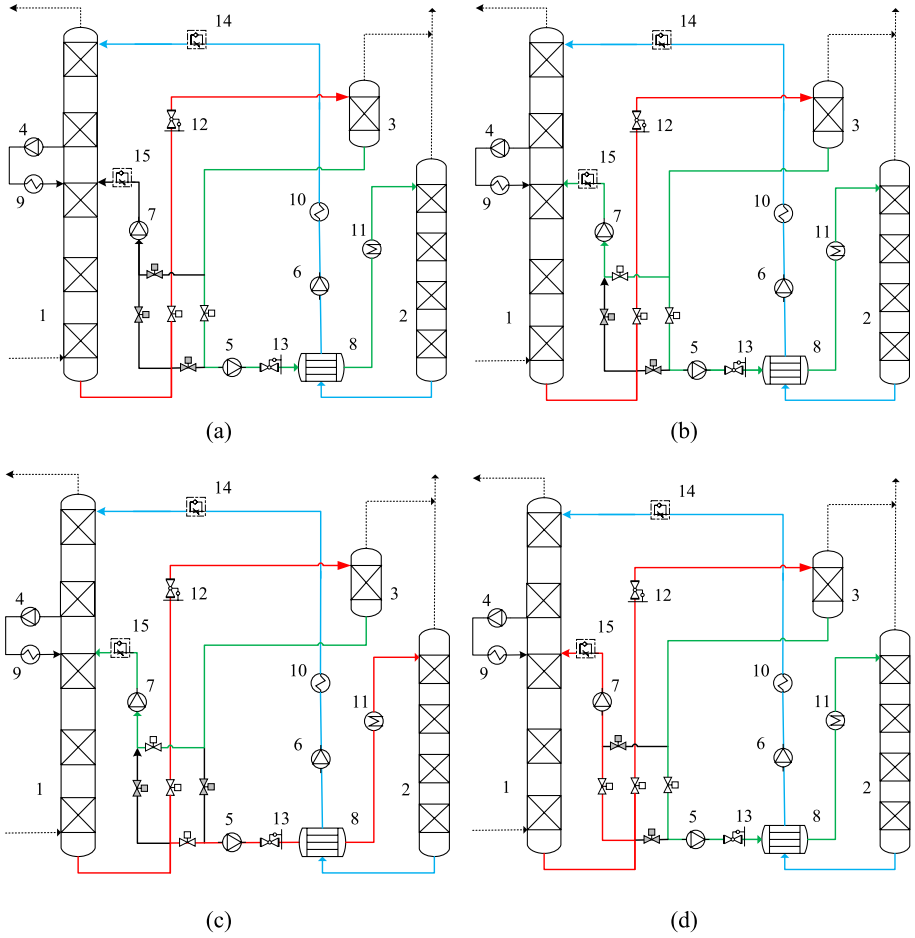

Fig. 15. Schematic diagram of process modification routes: (a) Route 1; (b) Route 2; (c) Route 3; and (d) Route 4. 1: absorber; 2: stripper; 3: flash evaporator; 4: intercooling pump; 5: rich solution pump; 6: lean solution pump; 7: semi-lean solution pump; 8: heat exchanger; 9: intercooler; 10: lean solution cooler; 11: pre-heater; 12: regulating valve; 13: pressure-reducing valve; 14: check valve.

cyclic capacity and a corresponding reduction in the regeneration energy compared with the 5 % split ratio. However, when the split ratio reached 20 %, the semi-lean solution flow rate became too low, significantly reducing CO_2 removal efficiency. To compensate for this, additional heating power was required, resulting in an increased regeneration energy.

Under Route 1, the regeneration energy was higher for MEA (2.41 GJ/t CO_2) than for MAA (1.78 GJ/t CO_2). Under Route 2, with an optimal split ratio of 10 %, the regeneration energy remained higher for MEA (2.44 GJ/t CO_2) than MAA (1.75 GJ/t CO_2). Adding SSR to Route 2 resulted in different outcomes; for MEA, Route 1 was more efficient than Route 2, whereas, for MAA, Route 2 was marginally more efficient than Route 1. Based on these results, Routes 1 and 2 showed no significant differences in performance under the optimal split ratios. Compared to Route 1, the positive effect of Route 2 improved rich solution loading and reduced lean solution flow, whereas its negative effects included increased cyclic capacity requirements and reduced semi-lean solution temperatures. In comparison, using only the AIC process, without any additional energy-saving strategies, resulted in a regeneration energy of 1.81 GJ/t CO_2 for MAA and 2.56 GJ/t CO_2 for MEA. Route 1 reduced the regeneration energies of MAA and MEA by 1.66 % and 5.86 %, respectively. In comparison, Route 2 achieved greater energy savings for MAA (3.32 %) but lower savings for MEA (4.69 %).

Route 3 achieved energy savings by recycling the semi-lean solution in the middle of the absorber (Fig. 15**(c)**). This approach reduced the flow rate of the rich solution entering the stripper while partially increasing the rich solution loading via the recycled semi-lean solution, thereby decreasing the requirement to reduce the lean solution loading. Consequently, the required input power decreased and the lower solution flow rate entering the stripper further reduced regeneration energy. The regeneration energy of Route 3 varied with the split ratio (Fig. 16 **(b)**); at a split ratio of zero, Route 3 corresponded to the conventional thermal desorption discussed in Section 3.2 (only AIC). With an increasing split ratio, the regeneration energy first decreased and then increased. This trend occurred because recycling a small fraction (5–15 %) of the rich solution by flashing it back into the absorber lowered the absorber temperature and enhanced CO_2 absorption, thereby increasing rich solution loading. Unlike Route 2, in which a larger portion of the rich solution bypasses the flashing stage, the majority of the solution under Route 3 enters the stripper directly, maintaining a higher rich solution temperature. During the experiments, the pre-heater was operated at the same power, preheating the rich solution to 88–92 °C. This setup isolated the effects of variations in the rich solution temperature on the regeneration energy. When the split ratio reached 20 %, the lean solution flow rate decreased significantly, requiring a higher regeneration heating power and increased regeneration energy. At the optimal split ratio of 10 %, the regeneration energy under Route 3 was MEA (2.38 GJ/t CO_2) > MAA (1.71 GJ/t CO_2), achieving energy savings of 5.52 % for MAA.

The variation in regeneration energy with split ratio was evaluated using Route 4 (Fig. 15**(d)**). Route 4 corresponds to Route 1 when the split ratio is zero. The regeneration energy for MAA and MEA increased with fluctuations as the split ratio increased, indicating that Route 4 offered less energy saving than Route 1 (Fig. 16**(c)**). Route 4 adds RSR to

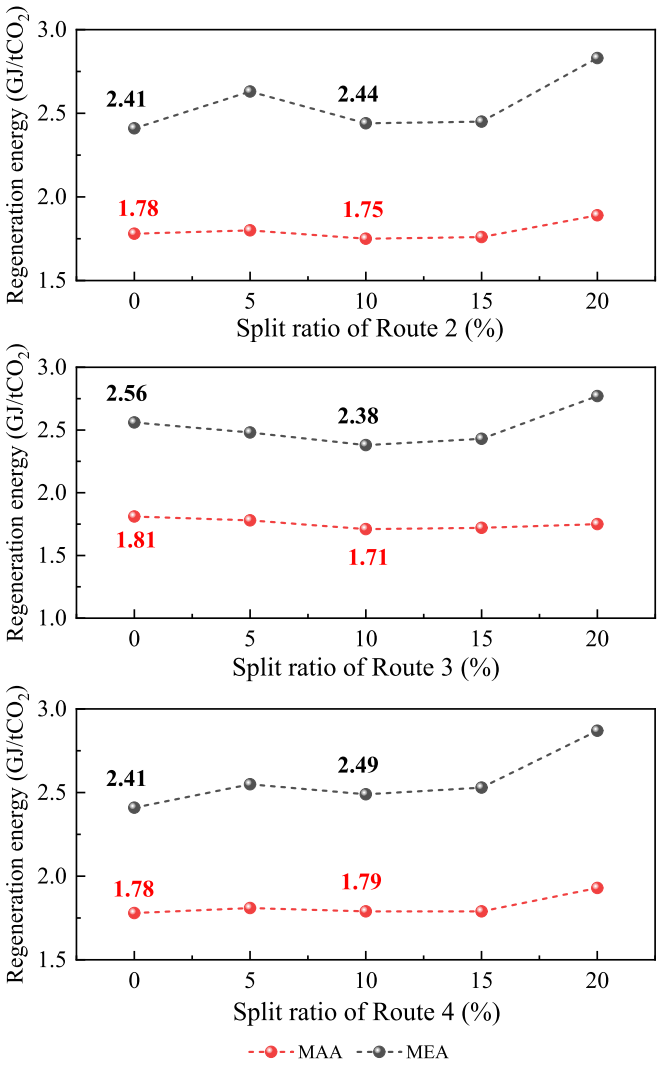

Fig. 16. Variation of regeneration energy with the split ratio for different routes in TGR-OBF gas tests.

Route 1; however, the recycled portion bypasses the flashing stage and its CO_2 loading remains relatively high. This limited the improvement in rich solution loading and primarily lowered the temperature in the middle section of the absorber. As the split ratio increased, the flow rate of the semi-lean solution entering the stripper decreased significantly, increasing the cyclic capacity requirements. Under Route 4, the optimal split ratio was 10 % and the regeneration energy was MEA (2.49 GJ/t CO_2) > MAA (1.79 GJ/t CO_2). The energy savings were 1.11 % for MAA and 2.73 % for MEA.

Under the pilot plant test conditions, all four process modifications resulted in energy savings compared with using only AIC (Table 5). Route 4 exhibited the lowest energy-saving effect, whereas Routes 1 and 2 showed no significant differences. Route 3 demonstrated the highest energy savings for MAA (5.52 %) and MEA (7.03 %). This outcome can be attributed to the fact that under Routes 1 and 2, a substantial portion of the rich solution underwent flashing, leading to a reduction in temperature in the flash evaporator and along the pipelines. Consequently, the regeneration energy was higher than that under Route 3. For larger-scale CO_2 capture systems, where heat loss from the equipment is less pronounced and the stripper regeneration gas can potentially be used to heat the flash evaporator, all four process modification routes may have energy-saving potential. The relative performances of Routes 2 and 3 in terms of energy savings can also shift under such conditions. Under the pilot plant conditions, the process modification in which 10 % of the rich solution entered the flash evaporator for flashing, with the resulting semi-lean solution entirely recycled to the middle section of the absorber, and the remaining 90 % was directed to the stripper for regeneration, exhibited the lowest regeneration energy.

Table 5
Performance outcomes of process modification routes.

Route	MAA		MEA	
	Regeneration energy (GJ/t CO_2)	Energy-saving percentage	Regeneration energy (GJ/t CO_2)	Energy-saving percentage
Route 1	1.78	1.66 %	2.41	5.86 %
Route 2	1.75	3.32 %	2.44	4.69 %
Route 3	1.71	5.52 %	2.38	7.03 %
Route 4	1.79	1.11 %	2.49	2.73 %

MAA: an amine blend absorbent primarily composed of MDEA and AEP [32]; MEA: monoethanolamine.

3.4. Amine emission test

Fig. 17 illustrates the effect of AIC on the volatile amine emissions measured at the top of the absorber, the first-stage water scrubber, and the second-stage water scrubber. The two-stage water scrubbing process effectively controlled the amine emissions from the solvent. Taking MAA as an example, with AIC, amine emissions decreased from 244.27 to 92.61 mg/Nm^3 after the first-stage water scrubber, representing a reduction of 62.15 %. After the second-stage water scrubber, amine emissions further decreased to 8.37 mg/Nm^3, corresponding to a 96.57 % reduction. AIC also contributed to a reduction in amine emissions. For example, in the case of MEA, emissions from the absorber top were reduced from 369.17 to 319.35 mg/Nm^3 with intercooling, achieving a 13.5 % reduction. The levels of amine emissions followed the order MEA > MAA.

The volatile amine emissions measured at the absorber, first-stage water scrubber, and second-stage water scrubber under the optimal TGR-OBF gas test operating conditions (Route 3, 10 % split ratio) were compared with those under the optimal BF gas test operating conditions. As shown in Fig. 18, the two-stage water scrubbing process effectively controlled the amine emissions in the TGR-OBF gas tests. For instance, in the case of MAA, amine emissions were reduced from 269.35 to 94.72 mg/Nm^3 after the first-stage water scrubber, representing a 62.15 %

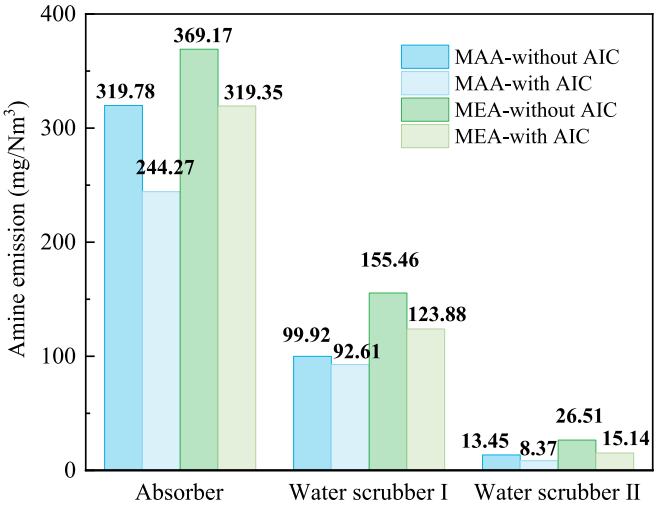

Fig. 17. Impact of AIC on amine emissions.

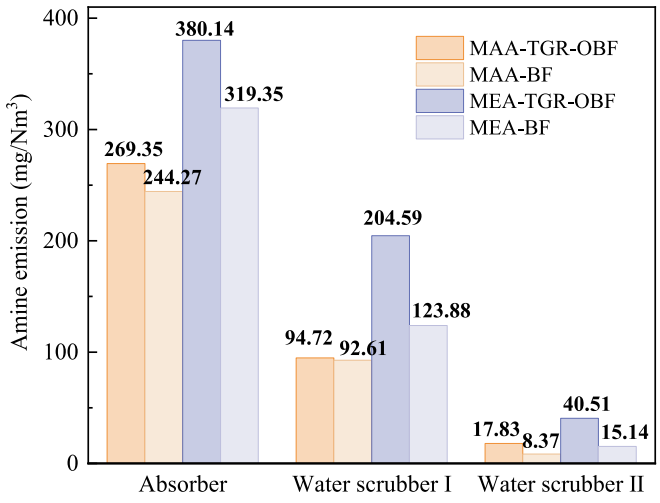

Fig. 18. Amine emission comparison between BF and TGR-OBF conditions.

reduction. After the second-stage water scrubber, amine emissions were further reduced to 17.83 mg/Nm^3, a 93.38 % reduction. However, compared to the BF tests, the TGR-OBF tests resulted in increased amine emissions. For example, the amine emissions of MAA at the top of the absorber during the TGR-OBF tests were 10.27 % higher than those in the BF tests. Under TGR-OBF conditions, with AIC and the Route 3 process modification, the amine emissions after two-stage water scrubbing were 17.83 mg/Nm^3 for MAA and 40.51 mg/Nm^3 for 30 % MEA.

4. Conclusion

Pilot tests on CO_2 capture from simulated BF and TGR-OBF gases were conducted using an MAA solvent and 30 wt% MEA, with the solvents operating stably for over 200 h. For BF gas, the lowest regeneration energy for MAA was 2.47 GJ/t CO_2 at an L/G of 8 L/Nm^3, while that for MEA of 3.78 GJ/t CO_2 was achieved at an L/G ratio of 10 L/Nm^3. The regeneration energy of MAA was 34.66 % lower than that of MEA. For TGR-OBF gas, MAA achieved a minimum regeneration energy of 1.81 GJ/t CO_2, a 26.72 % reduction compared to BF gas tests.

AIC had a significant effect on MAA, reducing the regeneration energy by up to 8.86 %. Under the TGR-OBF gas pilot test conditions, the lowest regeneration energy was achieved with a 10 % split ratio (Route 3), reducing the MAA regeneration energy by 5.52 %. These findings provide a clear pathway for improving the energy efficiency of industrial-scale CO_2 capture systems.

AIC effectively reduced amine emissions, although TGR-OBF gas testing resulted in higher amine emissions than BF gas testing. Two-stage water scrubbing effectively controlled solvent amine emissions, with MAA emissions reduced to 17.83 mg/Nm^3 after the second-stage water scrubber, demonstrating the feasibility of controlling solvent losses in large-scale applications.

The results highlight the potential of MAA as a highly efficient solvent for CO_2 capture in the steel industry. This study contributes to low-carbon steelmaking, a critical step toward achieving global climate goals. Moreover, the methodologies and findings can serve as a reference for optimizing CO_2 capture systems in other high-emission sectors.

CRediT authorship contribution statement

Ying Xie: Writing – review & editing, Writing – original draft, Visualization, Validation, Resources, Methodology, Investigation, Data curation, Conceptualization. **Zhixiang Xia:** Supervision, Investigation. **Chao Li:** Supervision, Investigation. **Man Mou:** Investigation. **Ximing Hu:** Supervision, Investigation. **Wei Chen:** Supervision, Investigation. **Xiaoming Xu:** Supervision, Funding acquisition. **Yang Xia:** Supervision, Funding acquisition. **Zihao Liu:** Supervision, Funding acquisition. **Mengxiang Fang:** Writing – review & editing, Methodology, Funding acquisition, Conceptualization.

Declaration of competing interest

The authors declare that they have no known competing financial interests or personal relationships that could have appeared to influence the work reported in this paper.

Acknowledgements

This work was supported by the National Key R&D Program of China (2023YFE0199300), the Pioneer R&D Program of Zhejiang Province (2022C03040), the Fundamental Research Funds for the Central Universities of China (2022ZFJH004), and a cooperation project from the Wuhan City Environment Protection Engineering Limited Company.

Data availability

Data will be made available on request.

References

[1] J. Perpiñán, B. Peña, M. Bailera, V. Eveloy, P. Kannan, A. Raj, P. Lisbona, L. M. Romeo, Integration of carbon capture technologies in blast furnace based steel making: A comprehensive and systematic review, Fuel 336 (2023) 127074, https://doi.org/10.1016/j.fuel.2022.127074.
[2] L. Ren, S. Zhou, T. Peng, X. Ou, A review of CO2 emissions reduction technologies and low-carbon development in the iron and steel industry focusing on China, Renew. Sustain. Energy Rev. 143 (2021) 110846, https://doi.org/10.1016/j.rser.2021.110846.
[3] X. Zhang, K. Jiao, J. Zhang, Z. Guo, A review on low carbon emissions projects of steel industry in the World, J. Clean. Prod. 306 (2021) 127259, https://doi.org/10.1016/j.jclepro.2021.127259.
[4] Z. Zhang, S. Hong, C. Lee, Role and impact of wash columns on the performance of chemical absorption-based CO2 capture process for blast furnace gas in iron and steel industries, Energy 271 (2023) 127020, https://doi.org/10.1016/j.energy.2023.127020.
[5] G.T. Rochelle, Amine Scrubbing for CO 2 Capture, Science (80-,) 325 (2009) 1652–1654, https://doi.org/10.1126/science.1176731.
[6] Á.A. Ramírez-Santos, C. Castel, E. Favre, A review of gas separation technologies within emission reduction programs in the iron and steel sector: Current application and development perspectives, Sep. Purif. Technol. 194 (2018) 425–442, https://doi.org/10.1016/j.seppur.2017.11.063.
[7] M.T. Ho, A. Bustamante, D.E. Wiley, Comparison of CO2 capture economics for iron and steel mills, Int. J. Greenh. Gas Control 19 (2013) 145–159, https://doi.org/10.1016/j.ijggc.2013.08.003.
[8] M. Abdul Quader, S. Ahmed, S.Z. Dawal, Y. Nukman, Present needs, recent progress and future trends of energy-efficient Ultra-Low Carbon Dioxide (CO2) Steelmaking (ULCOS) program, Renew. Sustain. Energy Rev. 55 (2016) 537–549, https://doi.org/10.1016/j.rser.2015.10.101.
[9] M. Pérez-Fortes, J.A. Moya, K. Vatopoulos, E. Tzimas, CO2 capture and utilization in cement and iron and steel industries, Energy Procedia 63 (2014) 6534–6543, https://doi.org/10.1016/j.egypro.2014.11.689.
[10] L. Hooey, A. Tobiesen, J. Johns, S. Santos, Techno-economic study of an integrated steelworks equipped with oxygen blast furnace and CO2 capture, Energy Procedia 37 (2013) 7139–7151, https://doi.org/10.1016/j.egypro.2013.06.651.
[11] M. Sundqvist, M. Biermann, F. Normann, M. Larsson, L. Nilsson, Evaluation of low and high level integration options for carbon capture at an integrated iron and steel mill, Int. J. Greenh. Gas Control 77 (2018) 27–36, https://doi.org/10.1016/j.ijggc.2018.07.008.
[12] J. Godin, W. Liu, S. Ren, C.C. Xu, Advances in recovery and utilization of carbon dioxide: A brief review, J. Environ. Chem. Eng. 9 (2021) 105644, https://doi.org/10.1016/j.jece.2021.105644.
[13] O. Khalifa, I.I.I. Alkhatib, D. Bahamon, A. Alhajaj, M.R.M. Abu-Zahra, L.F. Vega, Modifying absorption process configurations to improve their performance for post-combustion CO2 capture – what have we learned and what is still Missing? Chem. Eng. J. 430 (2022) 133096 https://doi.org/10.1016/j.cej.2021.133096.
[14] X.Y.D. Soo, J.J.C. Lee, W. Wu, L. Tao, C. Wang, Q. Zhu, J. Bu, Advancements in CO2 capture by absorption and adsorption: A comprehensive review, J. CO2 Util. 81 (2024) 102727, https://doi.org/10.1016/j.jcou.2024.102727.
[15] F.O. Ochedi, J. Yu, H. Yu, Y. Liu, A. Hussain, Carbon dioxide capture using liquid absorption methods: a review, Environ. Chem. Lett. 19 (2021) 77–109, https://doi.org/10.1007/s10311-020-01093-8.
[16] W. Jiang, Y. Lin, C. Sun, Y. Sun, Y. Zhu, Comparative review for enhancing CO2 capture efficiency with mixed amine systems and catalysts, Molecules 29 (2024) 4618, https://doi.org/10.3390/molecules29194618.

[17] N. El Hadri, D.V. Quang, E.L.V. Goetheer, M.R.M. Abu Zahra, Aqueous amine solution characterization for post-combustion CO2 capture process, Appl. Energy 185 (2017) 1433–1449, https://doi.org/10.1016/j.apenergy.2016.03.043.
[18] S. Ma'mun, H.F. Svendsen, K.A. Hoff, O. Juliussen, Selection of new absorbents for carbon dioxide capture, Energy Convers. Manag. 48 (2007) 251–258, https://doi.org/10.1016/j.enconman.2006.04.007.
[19] N. Khallaghi, S.Z. Abbas, G. Manzolini, E. De Coninck, V. Spallina, Techno-economic assessment of blast furnace gas pre-combustion decarbonisation integrated with the power generation, Energy Convers. Manag. 255 (2022) 115252, https://doi.org/10.1016/j.enconman.2022.115252.
[20] P. Jin, Z. Jiang, C. Bao, Y. Lu, J. Zhang, X. Zhang, Mathematical modeling of the energy consumption and carbon emission for the oxygen blast furnace with top gas recycling, Steel Res. Int. 87 (2016) 320–329, https://doi.org/10.1002/srin.201500054.
[21] G. Puxty, R. Rowland, A. Allport, Q. Yang, M. Bown, R. Burns, M. Maeder, M. Attalla, Carbon dioxide postcombustion capture: a novel screening study of the carbon dioxide absorption performance of 76 amines, Environ. Sci. Technol. 43 (2009) 6427–6433, https://doi.org/10.1021/es901376a.
[22] N. Yi, M. Fang, W. Di, Z. Xia, T. Wang, Q. Wang, Aerosol emissions of amine-based CO2 absorption system: effects of condensation nuclei and operating conditions, Environ. Sci. Technol. 55 (2021) 5152–5160, https://doi.org/10.1021/acs.est.0c04630.
[23] J. Perpiñán, M. Bailera, B. Peña, P. Kannan, V. Eveloy, L.M. Romeo, Power to gas and top gas recycling integration in an oxygen blast furnace steelmaking industry, J. CO2 Util. 78 (2023) 102634, https://doi.org/10.1016/j.jcou.2023.102634.
[24] B. Aghel, S. Janati, S. Wongwises, M.S. Shadloo, Review on CO2 capture by blended amine solutions, Int. J. Greenh. Gas Control 119 (2022) 103715, https://doi.org/10.1016/j.ijggc.2022.103715.
[25] M. Onoda, Y. Matsuzaki, F.A. Chowdhury, H. Yamada, K. Goto, S. Tonomura, Sustainable aspects of ultimate reduction of CO2 in the steelmaking process (COURSE50 Project), Part 2: CO2 Capture, J. Sustain. Metall. 2 (2016) 209–215, https://doi.org/10.1007/s40831-016-0067-3.
[26] K. Goto, H. Okabe, F.A. Chowdhury, S. Shimizu, Y. Fujioka, M. Onoda, Development of novel absorbents for CO2 capture from blast furnace gas, Int. J. Greenh. Gas Control 5 (2011) 1214–1219, https://doi.org/10.1016/j.ijggc.2011.06.006.
[27] J. Wells, A. Heeley, M. Akram, K.J. Hughes, D.B. Ingham, M. Pourkashanian, Simulation and modelling study of a chemical absorption plant to evaluate capture effectiveness when treating high CO2 content iron and steel industry emissions, Fuel 380 (2025) 133189, https://doi.org/10.1016/j.fuel.2024.133189.
[28] F.A. Tobiesen, H.F. Svendsen, T. Mejdell, Modeling of blast furnace CO2 capture using amine absorbents, Ind. Eng. Chem. Res. 46 (2007) 7811–7819, https://doi.org/10.1021/ie061556j.
[29] M. Dreillard, P. Broutin, P. Briot, T. Huard, A. Lettat, Application of the DMXTM CO2 Capture Process in Steel Industry, Energy Procedia 114 (2017) 2573–2589, https://doi.org/10.1016/j.egypro.2017.03.1415.
[30] W. Chung, K. Roh, J.H. Lee, Design and evaluation of CO2 capture plants for the steelmaking industry by means of amine scrubbing and membrane separation, Int. J. Greenh. Gas Control 74 (2018) 259–270, https://doi.org/10.1016/j.ijggc.2018.05.009.
[31] H. Li, Y. Zhao, C. Guo, J. Li, Analysis of technological pathways and development suggestions for blast furnace low-carbon ironmaking, Metals (basel). 14 (2024) 1276, https://doi.org/10.3390/met14111276.
[32] M. Fang, Y. Xie, Y. Shao, X. Xu, Y. Xia, M. Mou, X. Hu, T. Wang, Z. Liu, Development of carbon capture absorbents for top gas recycling-oxygen blast furnace in the steel industry, Sep. Purif. Technol. 355 (2025) 129616, https://doi.org/10.1016/j.seppur.2024.129616.
[33] S. Ji, X. Xu, Z. Jia, A system for removing CO2 from hydrogen rich carbon circulating blast furnace gas, CN 114456854 A, 2022.
[34] J. Choi, H. Cho, S. Yun, M.-G. Jang, S.-Y. Oh, M. Binns, J.-K. Kim, Process design and optimization of MEA-based CO2 capture processes for non-power industries, Energy 185 (2019) 971–980, https://doi.org/10.1016/j.energy.2019.07.092.
[35] K. Li, A. Cousins, H. Yu, P. Feron, M. Tade, W. Luo, J. Chen, Systematic study of aqueous monoethanolamine-based CO2 capture process: model development and process improvement, Energy Sci. Eng. 4 (2016) 23–39, https://doi.org/10.1002/ese3.101.
[36] A. Cousins, L.T. Wardhaugh, P.H.M. Feron, Preliminary analysis of process flow sheet modifications for energy efficient CO2 capture from flue gases using chemical absorption, Chem. Eng. Res. Des. 89 (2011) 1237–1251, https://doi.org/10.1016/j.cherd.2011.02.008.
[37] F. de Miguel Mercader, G. Magneschi, E. Sanchez Fernandez, G.J. Stienstra, E.L. V. Goetheer, Integration between a demo size post-combustion CO2 capture and full size power plant. An integral approach on energy penalty for different process options, Int. J. Greenh. Gas Control 11 (2012) S102–S113, https://doi.org/10.1016/j.ijggc.2012.09.016.
[38] T. Tu, X. Yang, Q. Cui, Y. Shang, S. Yan, CO2 regeneration energy requirement of carbon capture process with an enhanced waste heat recovery from stripped gas by advanced transport membrane condenser, Appl. Energy 323 (2022) 119593, https://doi.org/10.1016/j.apenergy.2022.119593.
[39] M. Stec, A. Tatarczuk, L. Więcław-Solny, A. Krótki, M. Ściążko, S. Tokarski, Pilot plant results for advanced CO2 capture process using amine scrubbing at the Jaworzno II Power Plant in Poland, Fuel 151 (2015) 50–56, https://doi.org/10.1016/j.fuel.2015.01.014.
[40] H. Ahn, M. Luberti, Z. Liu, S. Brandani, Process configuration studies of the amine capture process for coal-fired power plants, Int. J. Greenh. Gas Control 16 (2013) 29–40, https://doi.org/10.1016/j.ijggc.2013.03.002.
[41] L. Dubois, D. Thomas, Comparison of various configurations of the absorption-regeneration process using different solvents for the post-combustion CO2 capture applied to cement plant flue gases, Int. J. Greenh. Gas Control 69 (2018) 20–35, https://doi.org/10.1016/j.ijggc.2017.12.004.
[42] Z. Zhang, D.-N. Vo, J. Kum, S.-H. Hong, C.-H. Lee, Enhancing energy efficiency of chemical absorption-based CO2 capture process with advanced waste-heat recovery modules at a high capture rate, Chem. Eng. J. 472 (2023) 144918, https://doi.org/10.1016/j.cej.2023.144918.
[43] N.-S. Kwak, J. Jung, J. Lee, S.-C. Han, J.-G. Shim, K.-M. Kim, D.C. Lee, Field demonstration of a 10 MW CO2 capture pilot plant in extended operation using KoSol absorbents for treating off-gas in a coal fired power plant, Int. J. Greenh. Gas Control 135 (2024) 104134, https://doi.org/10.1016/j.ijggc.2024.104134.
[44] L. Dubois, D. Thomas, Simulations of various configurations of the post-combustion CO2 capture process applied to a cement plant flue gas: parametric study with different solvents, Energy Procedia 114 (2017) 1409–1423, https://doi.org/10.1016/j.egypro.2017.03.1265.
[45] Y. Le Moullec, M. Kanniche, Screening of flowsheet modifications for an efficient monoethanolamine (MEA) based post-combustion CO2 capture, Int. J. Greenh. Gas Control 5 (2011) 727–740, https://doi.org/10.1016/j.ijggc.2011.03.004.
[46] C. Nwaoha, P. Tontiwachwuthikul, Carbon dioxide capture from pulp mill using 2-amino-2-methyl-1-propanol and monoethanolamine blend: Techno-economic assessment of advanced process configuration, Appl. Energy 250 (2019) 1202–1216, https://doi.org/10.1016/j.apenergy.2019.05.097.